CHEMISTRY OF MATERIALS
Cite This: Chem. Mater. 2019, 31, 6889−6899
Article
pubs.acs.org/cm

Resilience to Conformational Fluctuations Controls Energetic Disorder in Conjugated Polymer Materials: Insights from Atomistic Simulations

Vincent Lemaur,[†] Jérôme Cornil,[†] Roberto Lazzaroni,[†] Henning Sirringhaus,[‡] David Beljonne,[†] and Yoann Olivier*[,†,⊥]

[†]Laboratory for Chemistry of Novel Materials, University of Mons, Place du Parc, 20, B-7000 Mons, Belgium
[‡]Cavendish Laboratory, University of Cambridge, JJ Thomson Avenue, Cambridge, CB3 0HE United Kingdom

Supporting Information

ABSTRACT: Increasing the crystallinity of thin films in concert with the planarization of the conjugated backbones has long been considered as the key for success in the design of polymer materials with optimized charge transport properties. Recently, this general belief had to be revisited with the emergence of a new class of disordered or even seemingly amorphous donor−acceptor conjugated polymers that exhibit charge mobilities larger than 1 $cm^2\ V^{-1}\ s^{-1}$. By combining all-atom molecular dynamics simulations to electronic structure calculations on three representative polymers, we demonstrate that high crystallinity and planar conjugated backbones are not mandatory to reach low-energetic-disorder materials. It is rather the resilience to thermal fluctuations of the torsions along the conjugated backbones within and between structural domains and the bulkiness of the alkyl side chains that control the energy landscape.

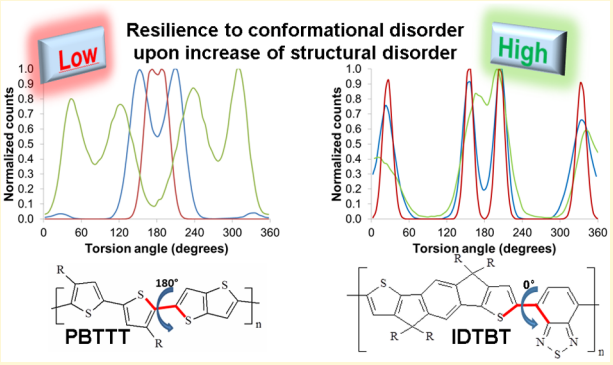

INTRODUCTION

The use of organic semiconductors in field-effect transistors has attracted growing interest and efforts in the last decades, which led to outstanding improvements in their performance. It is now common to find organic conjugated materials with room-temperature charge carrier mobility exceeding 1 $cm^2\ V^{-1}\ s^{-1}$.[1−5] Throughout the years, the highest values of the mobility were always reported for single crystals of organic small molecules such as pentacene, TIPS-pentacene, rubrene, [1]benzothieno[3,2-*b*]benzothiophene (BTBT), etc.[6−11] Those performances are often associated with the presence of delocalized states, as probed for instance by Hall effect measurements,[12−14] and properly accounted for by multiscale modeling.[15] Intensive work was therefore carried out in order to design molecular semiconductors achieving a high degree of order/crystallinity at the device scale.[11]

In contrast to small molecules, conjugated polymers often display limited long-range order, mainly due to their soft molecular nature giving rise to significant conformational freedom in both the backbone and the alkyl side-chain conformation. Consequently, polymer thin films are made of assemblies of microdomains, with a local organization varying from amorphous to crystalline. Efforts to improve the long-range charge transport properties in conjugated polymers were therefore aimed at increasing the presence of ordered/crystalline regions, i.e., obtaining semicrystalline materials. This can be triggered by tuning/tailoring the chemical structure of the monomer unit, the length and nature of the alkyl side chains, the processing techniques, etc.[16−24]

In semicrystalline materials, holes (electrons) are expected to mainly reside in the crystalline regions since they usually exhibit higher (lower)-lying (un)occupied HOMO (LUMO) levels in comparison to disordered regions. This is a result of solid-state packing effects, which often tend to limit the amplitude of the torsion of polymer segments away from planarity, thereby favoring charge carrier delocalization along the lamellae direction (i.e., stacking axis).[25] As a result of this energy barrier,[26] electrical connection between the crystalline regions is believed to occur through charge transport along polymer chains bridging different domains (often called "tie chains"[27,28]) and/or through chains within amorphous regions. Transport in the noncrystalline regions hampers the charge carrier mobility due to the increase in energetic disorder primarily driven by conformational disorder, which tends to promote charge localization.[29] The drop in mobility is, however, alleviated when using polymers with a high molecular

Special Issue: Jean-Luc Bredas Festschrift

Received: April 1, 2019
Revised: July 30, 2019
Published: July 30, 2019

DOI: 10.1021/acs.chemmater.9b01286
Chem. Mater. 2019, 31, 6889−6899

weight and large polydispersity, where the charges can percolate through the boundary regions.

For a long time, increasing the crystallinity of thin films in concert with the planarization of the conjugated backbones was thus thought to be key in the successful design of polymer materials with optimized charge transport properties. Recently, this general belief had to be revisited with the emergence of a new class of disordered or even seemingly amorphous organic conjugated polymers with a donor−acceptor type of structure that exhibits charge mobilities larger than 1 $cm^2\ V^{-1}\ s^{-1}$,[21,30−37] even when processed with low-cost manufacturing techniques such as spin coating. In contrast to semicrystalline polymers, these new polymers only exhibit short-range order (i.e., only local aggregation over a few chains in the π-stacking direction).[28,37,38] Based on the comparison of charge transport parameters (activation energies, paracrystallinity, energetic disorder, etc.) among more than 30 polymers, Noriega et al.[39] suggested that the key aspect to design high-mobility polymer materials is not to increase the crystallinity of the films but rather to increase their tolerance to disorder within the aggregates by allowing more efficient intra- and intermolecular charge transport at the segmental level. Later, Berggren et al.[28] tuned the local aggregation of poly(*N*,*N*′-bis-2-octyldodecyl-naphtalene-1,4,5,8-bis-dicarboximide-2,6-diyl-*alt*-5,5-2,2-bithiophene) (P(NDIOD2-T2)) chains from long-range to short-range ordering by blending with polystyrene. They demonstrated that aggregation over very few chains of P(NDIOD2-T2) is sufficient to ensure high electron mobility since the polymer chains retain locally the short-range intermolecular characteristics of a crystalline film and maintain an extended conformation ideal for connecting microdomains.

Venkateshvaran et al. measured the amount of energetic disorder in films of conjugated polymers going from semicrystalline to disordered morphologies through the study of the temperature dependence of the Seebeck coefficient in field-effect transistor architectures. They showed that a structurally highly disordered IDTBT copolymer (an indacenodithiophene-based copolymer with a benzathiadiazole fragment) surprisingly exhibits much lower energetic disorder and fewer electronic trap states than semicrystalline poly(2,5-bis(3-alkylthiophen-2-yl)thieno(3,2-*b*)thiophene) (PBTTT) or PSeDPPBT.[27] These results were confirmed with photothermal deflection spectroscopy measurements, from which Urbach energies were extracted, pointing to a small value for IDTBT (24 meV) compared to other copolymers:[40] 31 meV in P(NDIOD2-T2), 33 meV in DPPTTT, and 47 meV in PBTTT. Using a combination of molecular mechanics/molecular dynamics (MM/MD) to simulate phases of increasing disorder going from crystalline to the amorphous one for the same three polymers above and density functional theory calculations to obtain the density of states (DOS) in each phase, we have shown that the DOS broadening induced by side-chain disorder is in line with the measured Urbach energies.

Understanding at the atomistic level the fundamental reasons for the outstanding properties of such disordered polymers is thus crucial to better establish the link between microstructure and charge mobility values and ultimately design the next generation of conjugated polymers for field-effect transistors. In this context, we provide here a full atomistic microstructural description of PBTTT, P(NDIOD2-T2), and IDTBT, three state-of-the-art polymers (Figure 1), ranging from semicrystalline to disordered morphologies as

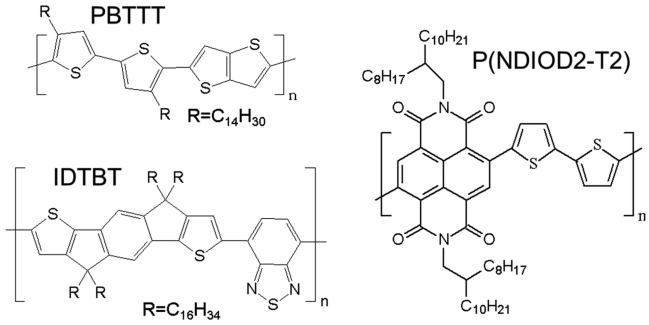

Figure 1. Chemical structures of PBTTT, P(NDIOD2-T2), and IDTBT.

well as in-depth characterization of their charge transport properties by characterizing both intra- and interchain charge transport. As a reference for a semicrystalline polymer, we consider PBTTT, a widely studied p-type polymer with hole mobilities reaching ∼1 $cm^2\ V^{-1}\ s^{-1}$. It is known to exhibit a high degree of crystallinity in thin films, with planar conjugated backbones.[41] The second structure under study is P(NDIOD2-T2), an n-type polymer with electron mobility up to ∼1 $cm^2\ V^{-1}\ s^{-1}$.[42] P(NDIOD2-T2) exhibits a moderate degree of crystallinity, but the chains are highly nonplanar compared to PBTTT: the torsion angle between the donor and acceptor fragments is ∼40°. Finally, we focus on the p-type IDTBT polymer, which exhibits high hole mobility (∼3 $cm^2\ V^{-1}\ s^{-1}$[37]) in spite of the absence of any long-range order between the chains. For all polymers, we have performed microstructural computational studies using MM/MD to simulate both crystalline and amorphous phases by controlling the degree of disorder among the alkyl side chains and among the polymer backbones.

In a second stage, we have carried out electronic structure calculations on isolated chains extracted from the morphologies generated with the MM/MD simulations, in order to get insights into the subtle interplay between the intrachain conformational disorder and the overall structural and energetic disorder that ultimately governs charge mobility. Here, we demonstrate that a high crystallinity and planar conjugated backbones are not mandatory to obtain materials with a low energetic disorder. It is rather the resilience to thermal fluctuations of the torsions along the conjugated backbones and the bulkiness of the alkyl side chains that control the density of states. In particular, our results indicate that hole transport in IDTBT proceeds predominantly along its polymer backbone and implies very few slow intermolecular charge hops, because of the absence of short contacts between the polymer backbones in the most disordered IDTBT phase. The remarkable charge transport properties of that polymer thus originate from the appropriate design of the chemical structure of the monomer unit, in particular the combination of electron-donating and -accepting units as well as the nature of the side chains.

■ MODELING STRATEGY

The strategy that we have used to generate thermodynamically stable crystalline structures consists in coupling molecular mechanics (MM) and molecular dynamics (MD) simulations on a unit cell containing a single chain with a limited number of monomer units (2 for IDTBT and 1 for P(NDIOD2-T2) and PBTTT) that is replicated using periodic boundary

DOI: 10.1021/acs.chemmater.9b01286
Chem. Mater. 2019, 31, 6889−6899

conditions to build a 3D infinite system. All MM/MD calculations have been performed with the Materials Studio (MS) 6.0 package using a force-field derived from Dreiding,[43] in which the torsion potentials between adjacent subunits and the torsions between the conjugated cores and the alkyl chains have been reparameterized and benchmarked against density functional theory (DFT) calculations using the B3LYP functional and the cc-pvtz basis set. The atomic charges have been obtained by fitting the electrostatic potential (ESP charges[44]) calculated at the B3LYP/cc-pvtz level on an isolated dimer. The conformational search procedure to extract the most stable supramolecular organizations involves four steps: (i) all starting structures (differing by the cell parameters, the relative orientations and positions of the conjugated cores and alkyl chains, the interdigitation of the alkyl chains, etc.) are optimized at the MM level; (ii) 100 ps-quenched MD runs (NPT, T = 300 K, quench frequency = 1 ps) are then performed on each optimized structure until the energy between two successive quenched systems no longer decreases; (iii) on the most stable structures obtained at step (ii), 100 ps-quenched MD runs are performed at higher temperature, successively at 600 K and 1000 K; and (iv) longer quenched simulations (t = 500 ps), using as starting points the most stable structure of the last quenched systems in step (iii), are performed at increasing temperature (300 K, 600 K, and 1000K) following the procedure developed in steps (ii) and (iii) to finally extract the most stable structure.

Larger periodic systems have then been built from the lowest energy structure to analyze the properties of the crystalline phase and to introduce disorder in a subsequent step. All systems are made of three layers of eight π-stacked ∼160 Å-long oligomers, i.e., 10 monomer units for IDTBT and 12 for P(NDIOD2-T2) and PBTTT. The structural and electronic properties of the crystalline phase are studied from 2 ns MD trajectories (NPT, P = 1 atm, T = 300 K) carried out after a 0.5 ns equilibration MD run.

In order to study the impact of increased structural disorder on the conformational and electronic properties of the assemblies, non-interdigitated and amorphous systems containing the same number of chains as the crystalline phase have also been considered. The non-interdigitated phase has been built from the crystalline phase in which the interlamellar distance has been increased up to 50 Å, so that the alkyl chains of successive layers are no longer interdigitated. After geometry optimization, the systems undergo a short (50 ps) MD simulation at high temperature (NPT, P = 1 atm, T = 500 K) to induce disorder along and between the polymer chains. A 500 ps-long MD simulation is then performed at room temperature (NPT, P = 1 atm, T = 300 K) to let the systems relax before running a last 2 ns-long acquisition MD run (NPT, P = 1 atm, T = 300 K) run, which is used for the analysis of the conformational and electronic properties of the non-interdigitated phase. The procedure used to generate the amorphous phases is the following: (i) 24 oligomers (decamers for IDTBT and dodecamers for PBTTT and P(NDIOD2-T2)) have been inserted randomly in a large unit cell (300 Å × 300 Å × 300 Å) and subjected to a 500 ps MD run at high temperature (NVT, T = 1000 K) while keeping the density low (∼0.02 g/cm^3) to favor a random spatial distribution of the oligomers; (ii) five successive 500 ps-long MD runs (NPT, P = 1 atm) were performed at decreasing temperature (1000 K, 500 K, 400 K, 350 K, 300 K); (iii) finally, a 2 ns-long MD simulation (NPT, P = 1 atm, T = 300 K) is performed and snapshots are saved every 5 ps for further analysis.

To characterize the supramolecular organization of the different systems, 400 snapshots have been recorded during the last 2 ns-long MD simulations. The torsional angle distribution profiles have been built from all torsions among all chains in the 400 snapshots. Note that all torsion angles ranging from 180° to 360° have been converted into the 0°−180° range. The torsion distribution profiles have been used to generate solid-state torsion potentials according to the Maxwell−Boltzmann law. The average deviations from planarity have been estimated as the average value of all torsion angles converted in the 0°−90° range. They are therefore different from the averaged torsion angle but much more insightful when discussing intramolecular charge transport since deviations from planarity play a key role in reducing delocalization of the charge carriers and their diffusion along the polymer chains. To characterize how chains are packed, the radial distribution functions between the different subunits have been built from the 400 snapshots, taking as reference point for each fragment the center of its central bond.

The electronic structure of isolated polymer chains, namely, IDTBT octamers and PBTTT and P(NDIOD2-T2) decamers extracted from the crystalline, non-interdigitated, and amorphous systems, has been calculated at the DFT level using the B3LYP functional and a 6-31G(d,p) basis set. The reported HOMO and LUMO energies are averaged over 100 snapshots, equally distributed over the 2 ns of the MD runs, for 10 randomly selected oligomers. To quantify the impact of structural disorder on the electronic properties, an energetic disorder parameter (σ_{tot}; $\sigma^2_{tot} = \sigma^2_{st} + \sigma^2_{dyn}$) has been calculated over 10 randomly selected molecules. It contains a dynamic part (σ_{dyn}), which reflects the fluctuation of the energy levels of individual chains over time, and a static part (σ_{st}) quantifying the deviation of the time-averaged energy levels. In practice, the dynamic contribution is estimated as the average over ten molecules of the standard deviations of the HOMO (or LUMO) energies associated with the 100 snapshots and the static part as the standard deviation of the time-averaged HOMO (or LUMO) level of the 10 molecules. A large dynamic disorder is expected to hamper intramolecular charge transport since it implies the collapse of extended states onto conformational segments, hence leading to a localization of the charge carriers. However, we note that dynamic disorder might be beneficial to intermolecular charge transport, provided that the transport operates in a hopping regime, by increasing the effective thermally averaged intermolecular hopping rate. Intermolecular charge transport is also strongly favored in materials with low static energetic disorder within the phase, since the excess charges would not encounter energetic steps acting as scattering or trap sites when hopping from chain to chain. High charge mobility would therefore be expected for materials with low static and dynamic energetic disorders.

In order to estimate the efficiency of intramolecular charge transport, effective masses corresponding to hole (electron) transport have been extracted from the curvature of the highest (lowest) electronic state of the valence (conduction) band. The band structure has been estimated from calculations for model systems at the DFT level using the B3LYP functional and a 6-31G(d,p) basis set where the unit cell (containing one (P(NDIOD2-T2) and PBTTT) or two (IDTBT) monomer unit(s)) was replicated in one direction to yield infinite

DOI: 10.1021/acs.chemmater.9b01286
Chem. Mater. 2019, 31, 6889−6899

isolated polymer chains. These monomer units are built in two steps: the central monomer unit(s) are first extracted from a fully DFT(B3LYP/6-31G(d,p))-optimized tetramer, and the torsion angles are then fixed, without further geometry optimization, at the average values of the torsion angles between the subunits in the different phases considered.

RESULTS AND DISCUSSION

Supramolecular Organization. We first discuss the supramolecular organization of the three polymers of interest, namely, PBTTT, P(NDIOD2-T2), and IDTBT. Since charge carriers are expected to travel in both ordered and disordered regions of thin films, we have generated phases with different degrees of order, going from crystalline to amorphous.[29,41,43−47] For each polymer, we first analyze the structural features of the most stable structure (referred to here as the crystalline structure) and how those features are modified upon a gradual increase in structural disorder (non-interdigitated and amorphous phases, see Modeling Strategy).

1° PBTTT. The most stable structure of PBTTT equipped with C_{14}-linear side chains exhibits a microsegregation between the conjugated cores and alkyl chains (see Figures 2 and SI1).

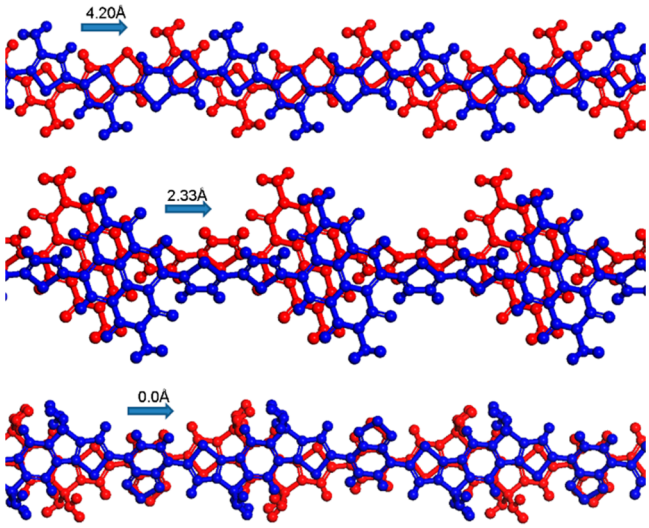

Figure 2. Representation of the organization of the conjugated cores of PBTTT (top), P(NDIOD2-T2) (center), and IDTBT (bottom) along the π-stacking direction in the crystalline phase. The amplitudes of the shifts of the chains along their long axes are shown by the arrows. The long alkyl chains have been removed for clarity.

The structural characteristics of our simulated structure fit quite well with experimental X-ray diffraction measurements.[48] The calculated interlamellar and π-stacking distances amount to 21.21 and 3.65 Å, respectively, compared to 21.2−21.5 and 3.7 Å measured experimentally for annealed films.[48] The relative position of the conjugated cores is, to a large extent, governed by the nature (linear versus branched) and number of the alkyl chains.[45,47] Because there are only two linear alkyl chains per monomer unit in PBTTT, neighboring molecules are mainly shifted along the long axis of the polymer chains to ensure a complete filling by alkyl side chains of the space between the conjugated cores of adjacent layers. The amplitude of that shift reaches 4.2 Å (~1/3 of the monomer length of 13.49 Å), in good agreement with previously reported data on the C_{12}−PBTTT derivative.[41] The conjugated backbones are planar in the crystalline phase, which implies that solid-state effects (i.e., intermolecular interactions) can overcome the ~1 kcal/mol energy barrier for planarization estimated from the DFT-calculated torsion potentials in the gas phase (see the black curves in Figure 3).

Inducing disorder within the alkyl chain regions, i.e., considering the non-interdigitated phase, maintains the lamellar structure and moderately impacts the supramolecular organization of the conjugated cores. In contrast, along the polymer chains, the alkyl chain disorder translates into a broadened torsion angle distribution, in particular between the thienothiophene and thiophene fragments. This originates from the absence of alkyl side chains on the thienothiophene unit, which allows for the full rotation of the thienothiophene with respect to its adjacent thiophene units (Figure 4). The deviation from planarity at the thienothiophene/thiophene connection increases from 13° ± 8° for the crystalline phase to 27° ± 15° for the non-interdigitated phase, while it only evolves from 6° ± 5° to 11° ± 8° for the torsion between the two substituted thiophene rings.

In the amorphous phase (see a snapshot in Figure 5), i.e., when introducing a high degree of disorder in both the alkyl and conjugated regions, we observe a considerable broadening of the torsion distributions along the polymer chains. Solid-state torsion potentials built by a Boltzmann inversion approach match quite well the DFT-calculated gas-phase torsion potentials (see Figure 3), reflecting the fact that polymer chains are only weakly interacting in the amorphous phase. Compared to the crystalline phase in which the polymer chains are shifted by ~4.2 Å along the polymer axis, the amorphous phase exhibits more face-to-face conformations of the polymer chains, as indicated by the increase in the radial distribution functions (rdf) at lower distances for donor−donor or acceptor−acceptor interactions, compared to donor−acceptor interactions (Figures 6 and SI2). This is most likely driven by one-to-one interactions between alkyl chains of neighboring PBTTT backbones. Figure 6 also shows a very broad peak at ~13.0 Å, which corresponds to the first-order intramolecular peak (i.e., the separation between the centers of mass of adjacent monomer units). The quite broad peak reflects a high flexibility of the polymer chains, which is also confirmed by a short average end-to-end distance (58 Å ± 17 Å in the amorphous phase) with respect to 160 Å for fully elongated chains (see Table SI1).

2° P(NDIOD2-T2). Previously, the simulated crystalline structure of the n-type P(NDIOD2-T2) polymer using a slightly different reparameterization scheme was reported.[45] Here, with our new force-field, we obtained very similar structural characteristics to those in ref 45, which, in all cases, are in good agreement with experimental X-ray diffraction results. The interlamellar spacing is well reproduced (25.1 Å versus 24.3−25.0 Å experimentally[49−51]), and the measured intense peak at 3.93 Å is described by simulated peaks ranging from 3.81 to 4.05 Å which correspond to contributions from both the conjugated cores and alkyl chains. The unit cell displayed in Figure SI2 shows that the dioctyl-dodecyl branched alkyl chains are interdigitated. In deep contrast to PBTTT, they do not adopt a fully extended conformation in order to better fill the space between two monomer units. Moreover, P(NDIOD2-T2) chains are only slightly shifted along both the long (2.33 Å) and the short (1.60 Å) polymer axis, thus leading to a microsegregation between electron-donating units (T2) and electron-accepting units (NDIOD2).

DOI: 10.1021/acs.chemmater.9b01286
Chem. Mater. 2019, 31, 6889−6899

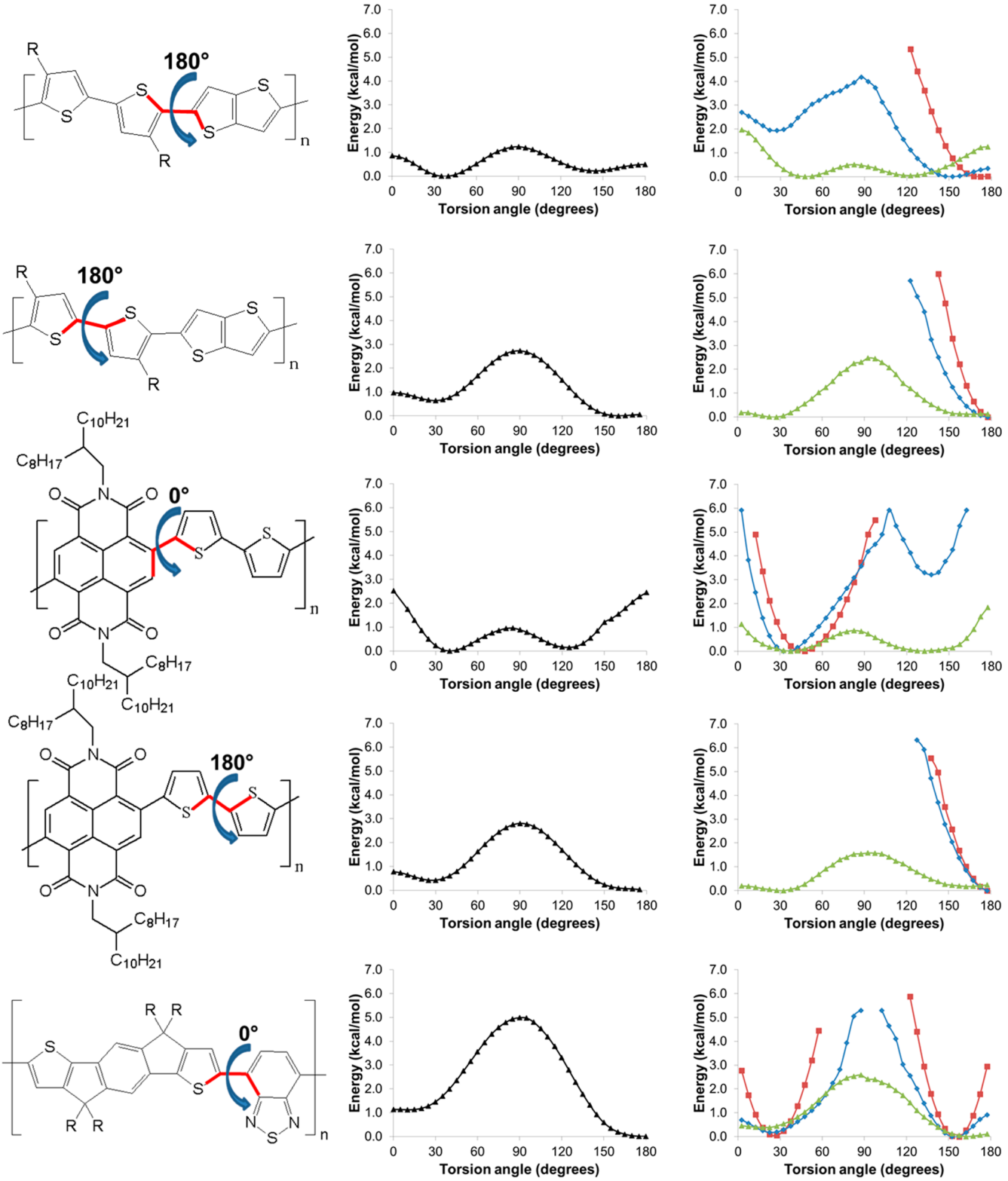

Figure 3. DFT-calculated (B3LYP/cc-pvtz) torsion potentials (black curves) corresponding to the torsion indicated in red (left panel) for an isolated monomer unit. The chosen angular references for the torsions are also indicated on the left panel. Right panel: inverted Boltzmann solid-state torsion potentials built from the analysis of the torsion angle distributions (see Figure 4) along all polymer chains and over 400 snapshots of the 2 ns MD runs for the crystalline (red), non-interdigitated (blue), and amorphous (green) systems (see Modeling Strategy).

This difference results from the fact that the P(NDIOD2-T2) conjugated backbones are twisted (~45° between the donor and acceptor segments for the anti-isomer[45]), which locks the chains along their backbone and makes translations very unlikely compared to planar chains.

The introduction of disorder among the alkyl side chains (non-interdigitated phase) has only a small impact on the

DOI: 10.1021/acs.chemmater.9b01286
Chem. Mater. 2019, 31, 6889−6899

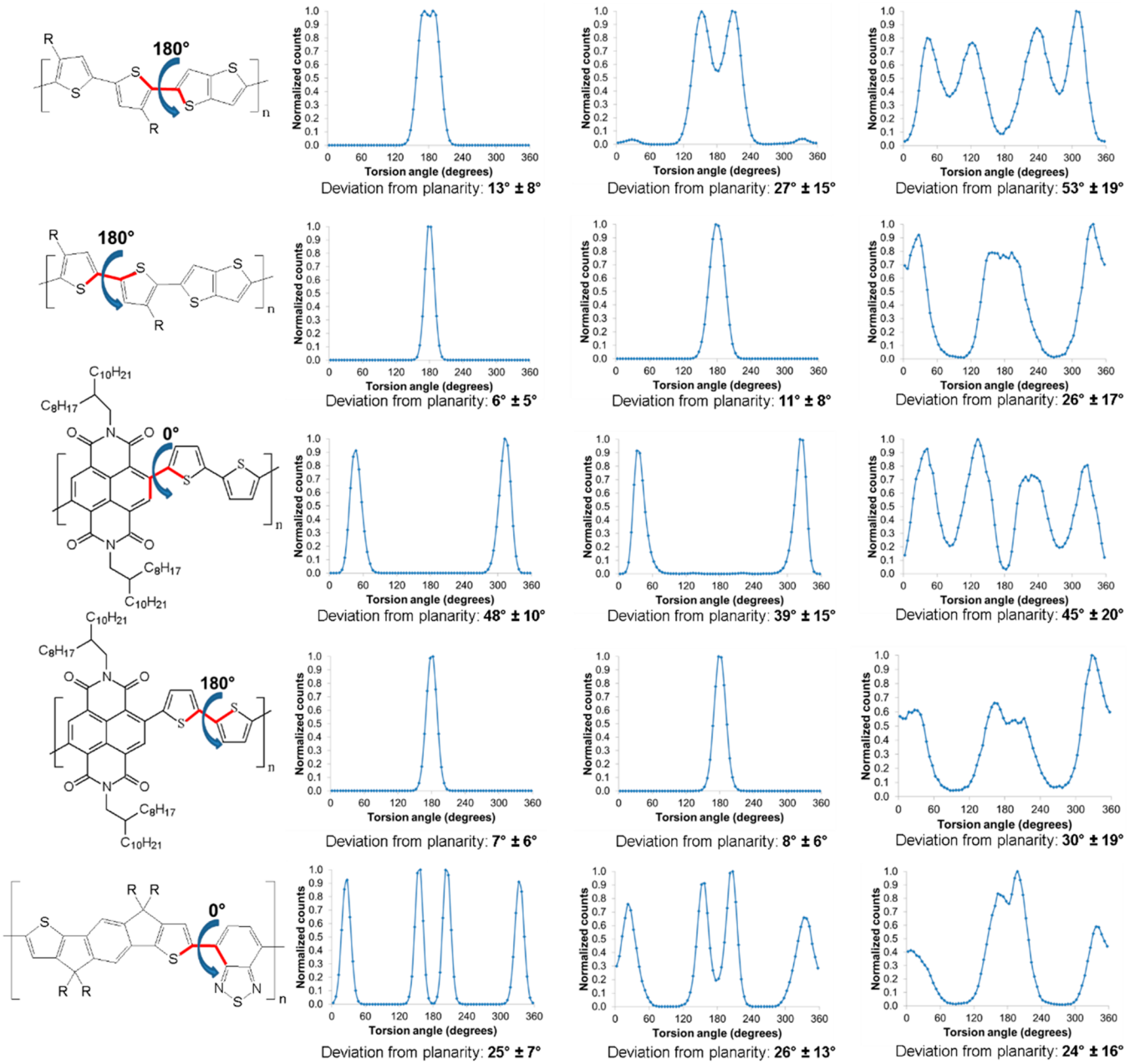

Figure 4. Calculated torsion distribution profiles of crystalline (left), non-interdigitated (center), and amorphous (right) systems built from the analysis of all torsions within all chains over the 400 snapshots of 2 ns MD runs. Note that all torsion angles ranging from 180° to 360° have been converted in the 0°−180° range. The averaged deviations from planarity and corresponding standard deviations have been estimated from the torsion angles converted in the 0°−90° range.

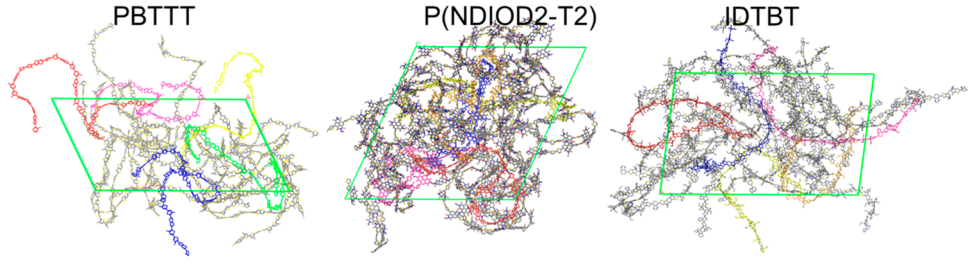

Figure 5. Representative snapshots of the simulated amorphous phase of PBTTT (left), P(NDIOD2-T2 (center), and IDTBT (right). All the hydrogens and carbons of the alkyl chains have been removed for clarity.

supramolecular assembly; the torsion angle distributions between the subunits are similar to those obtained for the crystalline phase (compare blue and red curves in Figure 3). Thus, P(NDIOD2-T2) is highly tolerant to side chain

DOI: 10.1021/acs.chemmater.9b01286
Chem. Mater. 2019, 31, 6889−6899

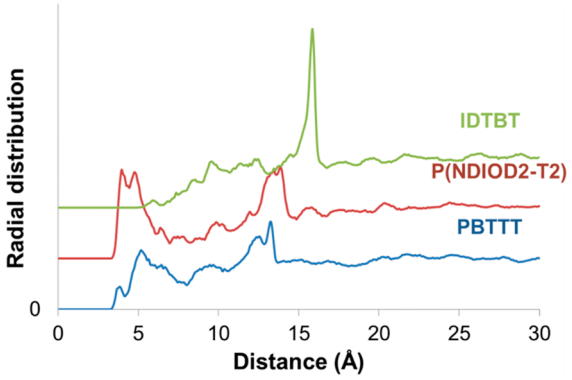

Figure 6. Radial distribution functions between the TT-TT subunits of PBTTT (blue), the NDIOD2-NDIOD2 subunits of P(NDIOD2-T2) (red), and the IDT-IDT subunits of IDTBT (green) in the amorphous states, as built from 400 snapshots saved during 2 ns MD runs. The reference point for each fragment is the center of their central covalent bond.

conformations, as we previously pointed out.[45] In contrast, in the amorphous phase, the thiophene−thiophene torsion is getting more flexible as a result of the weaker interaction between the side chains, with a deviation from planarity of 30° ± 19° (versus 7° ± 6° for the crystalline phase). Interestingly, while new maxima appear in the torsion distribution profile between the NDIOD2 and the thiophene units (corresponding to the syn-isomer[45]), the average deviation angle from planarity appears to be only slightly affected by the structural order of the phases (see Figure 4). This behavior is readily rationalized on the basis of the calculated torsion potentials. The energy cost for planarization of the thiophene−thiophene torsion is small and does not exceed 1 kcal/mol, while it reaches ∼3 kcal/mol for the donor−acceptor torsion (see Figure 3). The steeper torsion potential for the donor−acceptor torsion therefore prevents full planarization.

The rdf analysis (see Figures 6 and SI2) between the acceptor units clearly shows that specific interactions between NDIOD2 electron-accepting units are present in the amorphous phase; they tend to pack close to one another either by interactions between NDIOD2 units either from adjacent polymer chains or within the same polymer chain that tends to coil. This confirms the experimental evidence of the strong tendency of this polymer for aggregation.[52,53]

3° IDTBT. In the most stable structure of IDTBT (Figure 2), donor units (IDT) are lying on top of donors and acceptor units (BT) are lying on top of acceptors. In order to accommodate the two sets of two alkyl chains anchored on the 5-membered rings, the IDT fragments can only densely pack if they are oriented in opposite directions in adjacent chains (see Figure 2). The presence of two alkyl chains on each bridging carbon atom induces a significant bulkiness at the periphery of the conjugated IDT units and, as a consequence, gives rise to large π-stacking distances (∼4.7 Å). Since the equilibrium stacking distance between two isolated BT units is much smaller than 4.7 Å,[54] they rotate by 25° ± 7° with respect to the IDT units in the copolymer to get closer and maximize their stabilizing nonbonded interactions (i.e., van der Waals and electrostatic interactions), even though DFT-calculated torsion potentials predict that isolated chains would be planar. Since the energy cost for an 25° twist between the BT and IDT units with respect to the planar conformation is much below 1 kcal/mol, the energy barrier can be overcome during the stacking process, as also observed for P(NDIOD2-T2) and PBTTT.

Disorder within the alkyl chain regions has only a moderate impact on the organization of the conjugated cores even though the changes in the supramolecular arrangement translate into differences in the simulated X-ray diffraction patterns; a better agreement with experimental X-ray diffraction data is actually observed when introducing side-chain disorder.[37,40] The profiles of the torsion distributions in the crystalline and non-interdigitated phases are similar, with only a slight broadening of the peaks being observed (see Figure 4)—the conjugated backbones remain twisted.

In contrast to the first two polymers, the distribution of the torsion angles around the average equilibrium values of ∼25° in IDTBT is insensitive to the degree of intermolecular order; i.e., it is about the same in the crystalline versus amorphous phases. Very interestingly, the amount of planar chains is even increased in the amorphous phase, again showing that the torsion distributions in the amorphous phase compare well to DFT-calculated torsion potentials in the gas phase (15° ± 12°). The impact of the bulky side chains is less significant in the amorphous phase since they are only weakly interacting, as illustrated by the rdf analysis (see Figure 6). Indeed, the very few first IDT−IDT short contacts occur at a distance of ∼5 Å in the amorphous phase, and the probability to find donors at larger distances increases very slowly, reaching the density of an isotropic medium ($g(r) = 1$) for a distance of ∼12 Å. Note that the sharp character of the very intense peak at 15.9 Å, associated with an intramolecular distance (Figure SI2), reflects the high degree of intramolecular long-range order in this polymer (as compared to PBTTT or P(NDIOD2-T2), see Table SI1). The average end-to-end distance of the IDTBT chains is only reduced by 43% when going from crystalline to amorphous phases while the reduction amounts to 69% and 64% for P(NDIOD2-T2) and PBTTT, respectively.

To summarize this section, our calculations show that polymer chains behave in the amorphous phase as if they were not (or weakly) interacting. This is reflected by the solid-state torsion potentials built from the torsion population distributions, which are very similar to the DFT-calculated gas-phase torsion potentials. In contrast, the capacity of the conjugated cores to adopt a dense packing in the crystalline phase is essentially dictated by the nature (linear vs branched) and/or number of the alkyl side chains. A planarization of the conjugated backbone is systematically observed if three conditions are encountered: (i) the torsion potential is relatively flat; (ii) the chemical structure of the monomer unit favors close interactions; and (iii) the bulkiness and/or number of side chains do not hinder short contacts.

PBTTT exhibits a strong semicrystalline character because the chains can be easily planarized as a result of the relatively flat torsion potentials that, on the one hand, enable planarization in the crystalline phase and, on the other hand, yield a rather wide distribution of torsion angles in the amorphous phase. The less crystalline nature of the n-type P(NDIOD2-T2) arises from the steep torsion potential between the donor and the acceptor units and hence from huge energy cost to planarize the donor−acceptor connection. The rdf analysis clearly demonstrates the strong tendency of aggregation between the NDIOD2 units within one chain or between the chains. While IDTBT is expected to be planar based on the DFT-calculated torsion potentials, the bulkiness of the side chains induces large intermolecular distances in

DOI: 10.1021/acs.chemmater.9b01286
Chem. Mater. 2019, 31, 6889−6899

Table 1. Average Energy of the HOMO [LUMO] Levels of PBTTT [P(NDIOD2-T2)] Decamers and IDTBT Octamers in Their Crystalline, Non-interdigitated, and Amorphous Phases[a]

		energy (eV)	σ_{st} (meV)	σ_{dyn} (meV)	σ_{tot} (meV)	m^*
PBTTT (HOMO)	crystalline	−4.26	5	39	39	0.127
	noninterd	−4.33	23	45	51	0.141
	amorphous	−4.52	36	66	75	0.307
P(NDIOD2-T2) (LUMO)	crystalline	−3.83	4	40	40	0.356
	noninterd	−3.85	10	39	40	0.313
	amorphous	−3.89	25	63	68	0.352
IDTBT (HOMO)	crystalline	−4.37	4	38	38	0.103
	noninterd	−4.33	13	48	50	0.107
	amorphous	−4.19	33	44	55	0.141

[a]The static, dynamic, and total energetic disorders of each system are also listed in meV. The values are calculated from 10 randomly selected oligomers of each system over 100 snapshots extracted during 2 ns MD runs. The last column corresponds to the calculated effective mass.

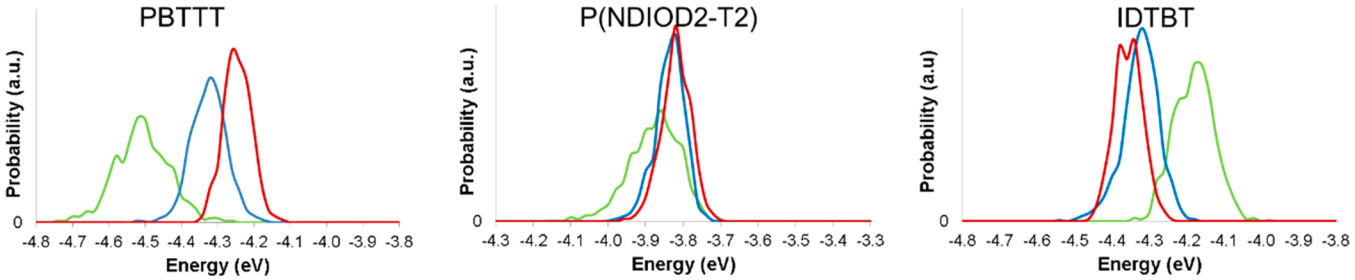

Figure 7. Representation of the HOMO [LUMO] distributions of PBTTT (left) [P(NDIOD2-T2 (center)] decamers and IDTBT (right) octamers in their crystalline (red), non-interdigitated (blue), and amorphous (green) phases.

ordered phases so that the BT electron-accepting units tend to twist with respect to the IDT electron-donating units in order to maximize intermolecular interactions. Interestingly, IDTBT gets more planar in the amorphous phase and recovers largely Boltzmann population characteristics of DFT-calculated torsion potentials on an isolated chain in the gas phase.

Electronic Structure Calculations. In this section, we resort to DFT electronic structure calculations: (i) to describe how the intramolecular and intermolecular degrees of freedom affect the energetic distribution experienced by charge carriers in finite-size models of the crystalline, non-interdigitated, and amorphous phases and (ii) to assess the propensity of the various polymers to transport charges along the polymer chains, by calculating the charge carrier effective masses in periodic systems frozen in the thermally averaged conformation for the three phases.

1° PBTTT. For PBTTT we only focus on the HOMO levels because of the p-type character of PBTTT. As expected from the torsional distribution analysis, the fluctuations in the average HOMO level energy are large for PBTTT when going from ordered to disordered phases. The significant increase in the equilibrium torsion angle from the crystalline to the amorphous phase translates into a stabilization of the HOMO level (increase in ionization potential) by up to 0.26 eV (see Table 1), due to the reduction in the degree of conjugation. Intermolecular hopping transport between domains made of different phases appears to be very unlikely in view of the limited overlap between the HOMO energy distributions in the amorphous and crystalline phases (see Figure 7). Besides, the amorphous phase shows a very broad energetic distribution owing to the large torsional disorder (see Table 1), which should limit intrachain hole diffusion, in line with recent experimental findings.[55] Overall, the large energy offset between ordered and disordered phases and the poor transport properties expected in the connecting disordered regions should result in holes that self-confine in the crystalline regions of the films with poor connectivity between the domains. This is consistent with the fact that the highest hole mobilities reported for this polymer are obtained for samples with the largest degree of crystallinity.[55] This is further supported by effective mass (m_h^*) calculations yielding small m_h^* values (0.127) for model polymer chains in the crystalline regions compared to disordered phases (0.307) (Table 1). The small m_h^* values in the crystalline phase match very well those calculated for other high-mobility polymers.[56,57]

2° P(NDIOD2-T2). For this polymer, we focus on electron transport. In contrast to PBTTT, the average energies of the LUMO level of P(NDIOD2-T2) are similar whatever the nature of the phase considered. These limited energetic fluctuations reflect the narrow distributions in torsion angles between the NDIOD2 and thiophene units along the polymer chains, irrespectively of the phase. Changes are only occurring for the thiophene−thiophene torsion angles, but their impact on electron transport is expected to be limited since the LUMO level is mainly localized on the NDIOD2 acceptors. Interestingly, while holes are expected to reside in the crystalline domains for PBTTT, electrons should not be strongly confined within specific domains in thin films of P(NDIOD2-T2). This is supported by recent experimental results[26] that show a tiny change in the bandgap when going from the crystalline to the amorphous phase (though it was found that the gap slightly widens in the amorphous phase, in contrast to the predictions from single-chain calculations, likely due to solid-state effects and dispersion not included in our model). Moreover, since the widths of the static disorder in each phase are the lowest among the different polymers under study (Table 1), intraphase intermolecular electron transport is expected to be the most efficient. Designing materials with

DOI: 10.1021/acs.chemmater.9b01286
Chem. Mater. 2019, 31, 6889−6899

equilibrium torsion angles that are independent of the degree of order in the phases is thus key to avoid charge trapping effects. The lack of long-range order in P(NDIOD2-T2) is not a drawback, especially in view of the strong tendency for aggregation of the NDIOD2 units, even in the amorphous phases, in concert with low static energetic disorder. On the one hand, intramolecular electron transport is not expected to be the dominant pathway in P(NDIOD2-T2) due to (i) the large calculated effective masses in all phases (between 0.313 and 0.356), similar to the values calculated for PBTTT for a highly twisted conformation corresponding to the amorphous phase, and (ii) the large dynamic energetic disorder. On the other hand, the large dynamic energetic disorder combined with large intermolecular transfer integrals for electron transport[45,58] and favorable NDIOD2 to NDIOD2 contacts indicate that electron transport in P(NDIOD2-T2) is mainly driven by intermolecular processes and hence is strongly affected by the very details of the supramolecular organization.

3° IDTBT. Similarly to PBTTT, IDTBT is a p-type semiconductor, so we focus here on hole transport. Very intriguingly, the HOMO level of IDTBT is shifted to higher energies (lower ionization potential) when going to disordered phases, in contrast with PBTTT and P(NDIOD2-T2). This peculiar behavior can be understood from the torsion distribution profiles, which show that an increase in the disorder within the phase tends to planarize some conjugated backbones as a result of the reduction of steric constraints. This results from the subtle interplay between bulkiness of the monomers and shape of the DFT-calculated torsion potentials. On one hand, in the gas phase (and therefore also in the weakly interacting amorphous phase), PBTTT is expected to be twisted while IDTBT is almost planar. On the other hand, in the crystalline phase, the strong aggregation of PBTTT chains leads to planarization of the conjugated segment while the bulkiness of the IDT donor segment hinders strong contacts between the BT accepting units which therefore twist with respect to the IDT moiety to get in closer contact. Together with the overlap between the HOMO energy distributions in the most ordered and amorphous phases (see Figure 7), this should ensure that most holes are mobile and do not get trapped spatially in the films. Even though the calculated static disorders are small in all phases, hole transport in IDTBT is essentially dominated by the intrachain contribution because of the large interchain distances (see Figure 7). The dominance of intrachain hole transport is consistent with the long persistence length observed experimentally[59] and in line with the structural calculations (i.e., end-to-end distances displaced toward the limit of fully extended chains and a sharp intramolecular peak in the rdf). The large hole mobility measured for this polymer is further supported both by the small effective masses computed in the different phases and by the smallest dynamic energetic disorder calculated among the amorphous phases of the different polymers. The latter feature has to be connected to the chemical structure of IDTBT, which presents the lowest number of torsions per unit length.

CONCLUSIONS

Based on a detailed analysis of the structural and electronic properties of workhorse p- and n-type conjugated polymers by means of combined molecular dynamics simulations and quantum-chemical electronic structure calculations, we have assessed the energy landscape for charge carriers in semi-crystalline and intrinsically disordered polymers. Our results show that high crystallinity of the materials and strict planarity of the polymer chains are not mandatory to get low-energetic-disorder polymers that promote high charge mobilities. A key factor governing charge transport is the resilience of the equilibrium torsion angle between ordered and disordered phases whatever its absolute value, thus implying that even twisted chains can efficiently transport charges. Whereas planar systems always promote efficient charge transport in crystalline domains, a dramatic drop of charge mobility is observed if the chains are no longer planar in disordered phases. The reason is twofold: (i) poor intermolecular charge transport is expected between the different domains due to the limited overlap between the energy distributions of the frontier orbitals causing large energy barrier between the crystalline and amorphous phases, and (ii) the decrease in conjugation length in disordered domains affects intramolecular charge transport by increasing the effective mass of the charge carriers.

Finally, we have highlighted that resilience to torsional disorder and hence an overall low energetic disorder could be achieved either by designing donor−acceptor copolymers with a steep torsion potential between adjacent fragments in the polymer chains (such as in P(NDIOD2-T2)) and/or, counterintuitively, by limiting intermolecular interactions by appropriate monomer design and/or side chain engineering to prevent the planarization of the chains in crystalline domains and make the torsional profiles similar in the different phases. Reducing the number of torsions per unit length also helps to ensure a long persistence length and hence to efficiently drive the charge carriers over long distances along the polymer backbone. Still, side chain engineering remains key in order to allow for the necessary short contacts in the most disordered regions of the films which prevent charge trapping. If these criteria are fulfilled, film crystallinity is clearly no longer the main parameter governing charge transport, which thus opens a new paradigm for the design of new high-mobility donor−acceptor copolymers.

ASSOCIATED CONTENT

Supporting Information

The Supporting Information is available free of charge on the ACS Publications website at DOI: 10.1021/acs.chemmater.9b01286.

Representation of the most stable unit cells of PBTTT, P(NDIOD2-T2), and IDTBT; radial distribution functions between among donors, acceptors, and donor−acceptor subunits of PBTTT, P(NDIOD2-T2), and IDTBT; and average end-to-end lengths and standard deviations of PBTTT, P(NDIOD2-T2), and IDTBT (PDF)

AUTHOR INFORMATION

Corresponding Author

*(Y.O.) E-mail: yoann.olivier@unamur.be.

ORCID

Jérôme Cornil: 0000-0002-5479-4227

Roberto Lazzaroni: 0000-0002-6334-4068

David Beljonne: 0000-0002-2989-3557

Present Address

⊥Theoretical and Structural Physical Chemistry Unit & Laboratoire de Physique du Solide, Namur Institute of

DOI: 10.1021/acs.chemmater.9b01286
Chem. Mater. 2019, 31, 6889−6899

Structured Matter, University of Namur, Rue de Bruxelles, 61, 5000 Namur, Belgium.

Notes

The authors declare no competing financial interest.

■ ACKNOWLEDGMENTS

The work in Mons was supported by the European Commission/Région Wallonne (FEDER − BIORGEL project), the Consortium des Équipements de Calcul Intensif (CÉCI), funded by the Fonds National de la Recherche Scientifique (F.R.S.-FNRS) under Grant No. 2.5020.11 as well as the Tier-1 supercomputer of the Fédération Wallonie-Bruxelles, infrastructure funded by the Walloon Region under Grant Agreement n1117545, and FRS-FNRS. The research in Mons is also funded through the European Union Horizon 2020 research and innovation program under Grant Agreement No. 646176 (EXTMOS project). J.C. and D.B. are FNRS Research Directors.

■ REFERENCES

(1) Li, Y.; Sonar, P.; Murphy, L.; Hong, W. High Mobility Diketopyrrolopyrrole (DPP)-Based Organic Semiconductor Materials for Organic Thin Film Transistors and Photovoltaics. *Energy Environ. Sci.* **2013**, *6* (6), 1684.

(2) Xie, W.; Frisbie, C. D. Electrolyte Gated Single-Crystal Organic Transistors to Examine Transport in the High Carrier Density Regime. *MRS Bull.* **2013**, *38* (01), 43−50.

(3) Sirringhaus, H. 25th Anniversary Article: Organic Field-Effect Transistors: The Path Beyond Amorphous Silicon. *Adv. Mater.* **2014**, *26* (9), 1319−1335.

(4) Wang, C.; Dong, H.; Hu, W.; Liu, Y.; Zhu, D. Semiconducting π-Conjugated Systems in Field-Effect Transistors: A Material Odyssey of Organic Electronics. *Chem. Rev.* **2012**, *112* (4), 2208−2267.

(5) Mas-Torrent, M.; Rovira, C. Role of Molecular Order and Solid-State Structure in Organic Field-Effect Transistors. *Chem. Rev.* **2011**, *111* (8), 4833−4856.

(6) Giri, G.; Verploegen, E.; Mannsfeld, S. C. B.; Atahan-Evrenk, S.; Kim, D. H.; Lee, S. Y.; Becerril, H. A.; Aspuru-Guzik, A.; Toney, M. F.; Bao, Z. Tuning Charge Transport in Solution-Sheared Organic Semiconductors Using Lattice Strain. *Nature* **2011**, *480* (7378), 504−508.

(7) Takeyama, Y.; Ono, S.; Matsumoto, Y. Organic Single Crystal Transistor Characteristics of Single-Crystal Phase Pentacene Grown by Ionic Liquid-Assisted Vacuum Deposition. *Appl. Phys. Lett.* **2012**, *101* (8), 083303.

(8) Braga, D.; Horowitz, G. High-Performance Organic Field-Effect Transistors. *Adv. Mater.* **2009**, *21* (14−15), 1473−1486.

(9) Yuan, Y.; Giri, G.; Ayzner, A. L.; Zoombelt, A. P.; Mannsfeld, S. C. B.; Chen, J.; Nordlund, D.; Toney, M. F.; Huang, J.; Bao, Z. Ultra-High Mobility Transparent Organic Thin Film Transistors Grown by an off-Centre Spin-Coating Method. *Nat. Commun.* **2014**, *5* (1), 3005.

(10) Schweicher, G.; Lemaur, V.; Niebel, C.; Ruzié, C.; Diao, Y.; Goto, O.; Lee, W.-Y.; Kim, Y.; Arlin, J.-B.; Karpinska, J. Bulky End-Capped [1]Benzothieno[3,2-b]Benzothiophenes: Reaching High-Mobility Organic Semiconductors by Fine Tuning of the Crystalline Solid-State Order. *Adv. Mater.* **2015**, *27* (19), 3066.

(11) Schweicher, G.; Olivier, Y.; Lemaur, V.; Geerts, Y. H. What Currently Limits Charge Carrier Mobility in Crystals of Molecular Semiconductors? *Isr. J. Chem.* **2014**, *54* (5−6), 595.

(12) Podzorov, V.; Menard, E.; Rogers, J. A.; Gershenson, M. E. Hall Effect in the Accumulation Layers on the Surface of Organic Semiconductors. *Phys. Rev. Lett.* **2005**, *95* (22), 226601.

(13) Yi, H. T.; Gartstein, Y. N.; Podzorov, V. Charge Carrier Coherence and Hall Effect in Organic Semiconductors. *Sci. Rep.* **2016**, *6* (1), 23650.

(14) Mitsui, C.; Okamoto, T.; Yamagishi, M.; Tsurumi, J.; Yoshimoto, K.; Nakahara, K.; Soeda, J.; Hirose, Y.; Sato, H.; Yamano, A.; et al. High-Performance Solution-Processable N-Shaped Organic Semiconducting Materials with Stabilized Crystal Phase. *Adv. Mater.* **2014**, *26* (26), 4546−4551.

(15) D'Avino, G.; Olivier, Y.; Muccioli, L.; Beljonne, D. Do Charges Delocalize over Multiple Molecules in Fullerene Derivatives? *J. Mater. Chem. C* **2016**, *4* (17), 3747−3756.

(16) McCulloch, I.; Heeney, M.; Bailey, C.; Genevicius, K.; MacDonald, I.; Shkunov, M.; Sparrowe, D.; Tierney, S.; Wagner, R.; Zhang, W.; et al. Liquid-Crystalline Semiconducting Polymers with High Charge-Carrier Mobility. *Nat. Mater.* **2006**, *5* (4), 328−333.

(17) Kim, B. J.; Lee, H.-S.; Lee, J. S.; Cho, S.; Kim, H.; Son, H. J.; Kim, H.; Ko, M. J.; Park, S.; Kang, M. S.; et al. Correlation between Crystallinity, Charge Transport, and Electrical Stability in an Ambipolar Polymer Field-Effect Transistor Based on Poly(Naphthalene- *Alt* -Diketopyrrolopyrrole). *J. Phys. Chem. C* **2013**, *117* (22), 11479−11486.

(18) Steyrleuthner, R.; Di Pietro, R.; Collins, B. A.; Polzer, F.; Himmelberger, S.; Schubert, M.; Chen, Z.; Zhang, S.; Salleo, A.; Ade, H.; et al. The Role of Regioregularity, Crystallinity, and Chain Orientation on Electron Transport in a High-Mobility n-Type Copolymer. *J. Am. Chem. Soc.* **2014**, *136* (11), 4245−4256.

(19) Hamadani, B. H.; Gundlach, D. J.; McCulloch, I.; Heeney, M. Undoped Polythiophene Field-Effect Transistors with Mobility of 1cm2V-1s-1. *Appl. Phys. Lett.* **2007**, *91* (24), 243512.

(20) Wang, S.; Kappl, M.; Liebewirth, I.; Müller, M.; Kirchhoff, K.; Pisula, W.; Müllen, K. Organic Field-Effect Transistors Based on Highly Ordered Single Polymer Fibers. *Adv. Mater.* **2012**, *24* (3), 417−420.

(21) Tsao, H. N.; Cho, D. M.; Park, I.; Hansen, M. R.; Mavrinskiy, A.; Yoon, D. Y.; Graf, R.; Pisula, W.; Spiess, H. W.; Müllen, K. Ultrahigh Mobility in Polymer Field-Effect Transistors by Design. *J. Am. Chem. Soc.* **2011**, *133* (8), 2605−2612.

(22) Crossland, E. J. W.; Tremel, K.; Fischer, F.; Rahimi, K.; Reiter, G.; Steiner, U.; Ludwigs, S. Anisotropic Charge Transport in Spherulitic Poly(3-Hexylthiophene) Films. *Adv. Mater.* **2012**, *24* (6), 839−844.

(23) Sirringhaus, H.; Brown, P. J.; Friend, R. H.; Nielsen, M. M.; Bechgaard, K.; Langeveld-Voss, B. M. W.; Spiering, A. J. H.; Janssen, R. A. J.; Meijer, E. W.; Herwig, P.; et al. Two-Dimensional Charge Transport in Self-Organized, High-Mobility Conjugated Polymers. *Nature* **1999**, *401* (6754), 685−688.

(24) Oosterbaan, W. D.; Bolsée, J.-C.; Wang, L.; Vrindts, V.; Lutsen, L. J.; Lemaur, V.; Beljonne, D.; McNeill, C. R.; Thomsen, L.; Manca, J. V. On the Relation between Morphology and FET Mobility of Poly(3- Alkylthiophene)s at the Polymer/SiO_2 and Polymer/Air Interface. *Adv. Funct. Mater.* **2014**, *24* (14), 1994.

(25) Zhao, N.; Noh, Y.-Y.; Chang, J.-F.; Heeney, M.; McCulloch, I.; Sirringhaus, H. Polaron Localization at Interfaces in High-Mobility Microcrystalline Conjugated Polymers. *Adv. Mater.* **2009**, *21* (37), 3759−3763.

(26) Statz, M.; Venkateshvaran, D.; Jiao, X.; Schott, S.; McNeill, C. R.; Emin, D.; Sirringhaus, H.; Di Pietro, R. On the Manifestation of Electron-Electron Interactions in the Thermoelectric Response of Semicrystalline Conjugated Polymers with Low Energetic Disorder. *Commun. Phys.* **2018**, *1* (1), 16.

(27) Broch, K.; Venkateshvaran, D.; Lemaur, V.; Olivier, Y.; Beljonne, D.; Zelazny, M.; Nasrallah, I.; Harkin, D. J.; Statz, M.; Pietro, R. D.; Kronemeijer, A. J.; Sirringhaus, H. Measurements of Ambipolar Seebeck Coefficients in High-Mobility Diketopyrrolopyrrole Donor-Acceptor Copolymers. *Adv. Electron. Mater.* **2017**, *3* (11), 1700225.

(28) Wang, S.; Fabiano, S.; Himmelberger, S.; Puzinas, S.; Crispin, X.; Salleo, A.; Berggren, M. Experimental Evidence That Short-Range Intermolecular Aggregation Is Sufficient for Efficient Charge Transport in Conjugated Polymers. *Proc. Natl. Acad. Sci. U. S. A.* **2015**, *112* (34), 10599−10604.

DOI: 10.1021/acs.chemmater.9b01286
Chem. Mater. 2019, 31, 6889−6899

(29) Liu, T.; Troisi, A. Understanding the Microscopic Origin of the Very High Charge Mobility in PBTTT: Tolerance of Thermal Disorder. *Adv. Funct. Mater.* **2014**, *24* (7), 925−933.
(30) Back, J. Y.; Yu, H.; Song, I.; Kang, I.; Ahn, H.; Shin, T. J.; Kwon, S.-K.; Oh, J. H.; Kim, Y.-H. Investigation of Structure−Property Relationships in Diketopyrrolopyrrole-Based Polymer Semiconductors via Side-Chain Engineering. *Chem. Mater.* **2015**, *27* (5), 1732−1739.
(31) Tang, W.; Li, J.; Zhao, J.; Zhang, W.; Yan, F.; Guo, X. High-Performance Solution-Processed Low-Voltage Polymer Thin-Film Transistors With Low-k/High-k Bilayer Gate Dielectric. *IEEE Electron Device Lett.* **2015**, *36* (9), 950−952.
(32) Han, A.-R.; Dutta, G. K.; Lee, J.; Lee, H. R.; Lee, S. M.; Ahn, H.; Shin, T. J.; Oh, J. H.; Yang, C. *ε* -Branched Flexible Side Chain Substituted Diketopyrrolopyrrole-Containing Polymers Designed for High Hole and Electron Mobilities. *Adv. Funct. Mater.* **2015**, *25* (2), 247−254.
(33) Baeg, K.-J.; Caironi, M.; Noh, Y.-Y. Toward Printed Integrated Circuits Based on Unipolar or Ambipolar Polymer Semiconductors. *Adv. Mater.* **2013**, *25* (31), 4210−4244.
(34) Lee, J.; Han, A.-R.; Kim, J.; Kim, Y.; Oh, J. H.; Yang, C. Solution-Processable Ambipolar Diketopyrrolopyrrole−Selenophene Polymer with Unprecedentedly High Hole and Electron Mobilities. *J. Am. Chem. Soc.* **2012**, *134* (51), 20713−20721.
(35) Mei, J.; Kim, D. H.; Ayzner, A. L.; Toney, M. F.; Bao, Z. Siloxane-Terminated Solubilizing Side Chains: Bringing Conjugated Polymer Backbones Closer and Boosting Hole Mobilities in Thin-Film Transistors. *J. Am. Chem. Soc.* **2011**, *133* (50), 20130−20133.
(36) Bronstein, H.; Chen, Z.; Ashraf, R. S.; Zhang, W.; Du, J.; Durrant, J. R.; Shakya Tuladhar, P.; Song, K.; Watkins, S. E.; Geerts, Y.; et al. Thieno[3,2- *b*]Thiophene-Diketopyrrolopyrrole-Containing Polymers for High-Performance Organic Field-Effect Transistors and Organic Photovoltaic Devices. *J. Am. Chem. Soc.* **2011**, *133* (10), 3272−3275.
(37) Zhang, X.; Bronstein, H.; Kronemeijer, A. J.; Smith, J.; Kim, Y.; Kline, R. J.; Richter, L. J.; Anthopoulos, T. D.; Sirringhaus, H.; Song, K.; et al. Molecular Origin of High Field-Effect Mobility in an Indacenodithiophene−benzothiadiazole Copolymer. *Nat. Commun.* **2013**, *4* (1), 2238.
(38) Zhang, W.; Smith, J.; Watkins, S. E.; Gysel, R.; McGehee, M.; Salleo, A.; Kirkpatrick, J.; Ashraf, S.; Anthopoulos, T.; Heeney, M.; et al. Indacenodithiophene Semiconducting Polymers for High-Performance, Air-Stable Transistors. *J. Am. Chem. Soc.* **2010**, *132* (33), 11437−11439.
(39) Noriega, R.; Rivnay, J.; Vandewal, K.; Koch, F. P. V.; Stingelin, N.; Smith, P.; Toney, M. F.; Salleo, A. A General Relationship between Disorder, Aggregation and Charge Transport in Conjugated Polymers. *Nat. Mater.* **2013**, *12* (11), 1038−1044.
(40) Venkateshvaran, D.; Nikolka, M.; Sadhanala, A.; Lemaur, V.; Zelazny, M.; Kepa, M.; Hurhangee, M.; Kronemeijer, A. J.; Pecunia, V.; Nasrallah, I. Approaching Disorder-Free Transport in High-Mobility Conjugated Polymers. *Nature* **2014**, *515* (7527), 384.
(41) Brocorens, P.; Van Vooren, A.; Chabinyc, M. L.; Toney, M. F.; Shkunov, M.; Heeney, M.; McCulloch, I.; Cornil, J.; Lazzaroni, R. Solid-State Supramolecular Organization of Polythiophene Chains Containing Thienothiophene Units. *Adv. Mater.* **2009**, *21* (10−11), 1193−1198.
(42) Yan, H.; Chen, Z.; Zheng, Y.; Newman, C.; Quinn, J. R.; Dötz, F.; Kastler, M.; Facchetti, A. A High-Mobility Electron-Transporting Polymer for Printed Transistors. *Nature* **2009**, *457* (7230), 679−686.
(43) Mayo, S. L.; Olafson, B. D.; Goddard, W. A. DREIDING: A Generic Force Field for Molecular Simulations. *J. Phys. Chem.* **1990**, *94* (26), 8897−8909.
(44) Besler, B. H.; Merz, K. M.; Kollman, P. A. Atomic Charges Derived from Semiempirical Methods. *J. Comput. Chem.* **1990**, *11* (4), 431−439.
(45) Lemaur, V.; Muccioli, L.; Zannoni, C.; Beljonne, D.; Lazzaroni, R.; Cornil, J.; Olivier, Y. On the Supramolecular Packing of High Electron Mobility Naphthalene Diimide Copolymers: The Perfect Registry of Asymmetric Branched Alkyl Side Chains. *Macromolecules* **2013**, *46* (20), 8171.
(46) Niedzialek, D.; Lemaur, V.; Dudenko, D.; Shu, J.; Hansen, M. R.; Andreasen, J. W.; Pisula, W.; Müllen, K.; Cornil, J.; Beljonne, D. Probing the Relation between Charge Transport and Supramolecular Organization down to Ångström Resolution in a Benzothiadiazole-Cyclopentadithiophene Copolymer. *Adv. Mater.* **2013**, *25* (13), 1939.
(47) Olivier, Y.; Niedzialek, D.; Lemaur, V.; Pisula, W.; Müllen, K.; Koldemir, U.; Reynolds, J. R.; Lazzaroni, R.; Cornil, J.; Beljonne, D. 25th Anniversary Article: High-Mobility Hole and Electron Transport Conjugated Polymers: How Structure Defines Function. *Adv. Mater.* **2014**, *26* (14), 2119.
(48) Chabinyc, M. L.; Toney, M. F.; Kline, R. J.; McCulloch, I.; Heeney, M. X-Ray Scattering Study of Thin Films of Poly(2,5-Bis(3-Alkylthiophen-2-Yl)Thieno[3,2- *b*]Thiophene). *J. Am. Chem. Soc.* **2007**, *129* (11), 3226−3237.
(49) Schuettfort, T.; Thomsen, L.; McNeill, C. R. Observation of a Distinct Surface Molecular Orientation in Films of a High Mobility Conjugated Polymer. *J. Am. Chem. Soc.* **2013**, *135* (3), 1092−1101.
(50) Rivnay, J.; Steyrleuthner, R.; Jimison, L. H.; Casadei, A.; Chen, Z.; Toney, M. F.; Facchetti, A.; Neher, D.; Salleo, A. Drastic Control of Texture in a High Performance N-Type Polymeric Semiconductor and Implications for Charge Transport. *Macromolecules* **2011**, *44* (13), 5246−5255.
(51) Rivnay, J.; Toney, M. F.; Zheng, Y.; Kauvar, I. V.; Chen, Z.; Wagner, V.; Facchetti, A.; Salleo, A. Unconventional Face-On Texture and Exceptional In-Plane Order of a High Mobility n-Type Polymer. *Adv. Mater.* **2010**, *22* (39), 4359−4363.
(52) Luzio, A.; Criante, L.; D'Innocenzo, V.; Caironi, M. Control of Charge Transport in a Semiconducting Copolymer by Solvent-Induced Long-Range Order. *Sci. Rep.* **2013**, *3*, 3425.
(53) Steyrleuthner, R.; Schubert, M.; Howard, I.; Klaumünzer, B.; Schilling, K.; Chen, Z.; Saalfrank, P.; Laquai, F.; Facchetti, A.; Neher, D. Aggregation in a High-Mobility n-Type Low-Bandgap Copolymer with Implications on Semicrystalline Morphology. *J. Am. Chem. Soc.* **2012**, *134* (44), 18303−18317.
(54) Cornil, J.; Gueli, I.; Dkhissi, A.; Sancho-Garcia, J. C.; Hennebicq, E.; Calbert, J. P.; Lemaur, V.; Beljonne, D.; Brédas, J. L. Electronic and Optical Properties of Polyfluorene and Fluorene-Based Copolymers: A Quantum-Chemical Characterization. *J. Chem. Phys.* **2003**, *118* (14), 6615.
(55) Vakhshouri, K.; Smith, B. H.; Chan, E. P.; Wang, C.; Salleo, A.; Wang, C.; Hexemer, A.; Gomez, E. D. Signatures of Intracrystallite and Intercrystallite Limitations of Charge Transport in Polythiophenes. *Macromolecules* **2016**, *49* (19), 7359−7369.
(56) Hsu, B. B.-Y.; Cheng, C.-M.; Luo, C.; Patel, S. N.; Zhong, C.; Sun, H.; Sherman, J.; Lee, B. H.; Ying, L.; Wang, M.; et al. The Density of States and the Transport Effective Mass in a Highly Oriented Semiconducting Polymer: Electronic Delocalization in 1D. *Adv. Mater.* **2015**, *27* (47), 7759−7765.
(57) Yuan, Z.; Fu, B.; Thomas, S.; Zhang, S.; DeLuca, G.; Chang, R.; Lopez, L.; Fares, C.; Zhang, G.; Bredas, J.-L.; et al. Unipolar Electron Transport Polymers: A Thiazole Based All-Electron Acceptor Approach. *Chem. Mater.* **2016**, *28* (17), 6045−6049.
(58) Wetzelaer, G.-J. A. H.; Kuik, M.; Olivier, Y.; Lemaur, V.; Cornil, J.; Fabiano, S.; Loi, M. A.; Blom, P. W. M. Asymmetric Electron and Hole Transport in a High-Mobility n-Type Conjugated Polymer. *Phys. Rev. B: Condens. Matter Mater. Phys.* **2012**, *86* (16), 165203.
(59) Vezie, M. S.; Few, S.; Meager, I.; Pieridou, G.; Dörling, B.; Ashraf, R. S.; Goñi, A. R.; Bronstein, H.; McCulloch, I.; Hayes, S. C.; et al. Exploring the Origin of High Optical Absorption in Conjugated Polymers. *Nat. Mater.* **2016**, *15* (7), 746−753.

DOI: 10.1021/acs.chemmater.9b01286
Chem. Mater. 2019, 31, 6889−6899